Journal of Materials, Processing and Design (2025)
Clausius Scientific Press, Canada

DOI: 10.23977/jmpd.2025.090110
ISSN 2516-0923 Vol. 9 Num. 1

Isothermal section of the Mn-Ni-Si ternary system at 500°C

Junyi Liang[1,2,a], Yongfa Zheng[1,2,b], Xuehong Cui[1,2,*]

[1]Guangxi Colleges and Universities Key Laboratory of Environmental Friendly Materials and Ecological Restoration, School of Materials, Guangxi Minzu University, Nanning, Guangxi, China
[2]Guangxi Key Laboratory of Advanced Structural Materials and Carbon Neutralization, School of Materials and Environment, Guangxi Minzu University, Nanning, Guangxi, China
[a]994327325@qq.com, [b]1634546707@qq.com
**Corresponding author: cxh841113@163.com*

Keywords: Mn-Ni-Si System; Phase Diagram; X-Ray Diffraction; Scanning Electron Microscopy

Abstract: The Mn-Ni-Si ternary system is an important ternary alloy system in the steel used for reactor pressure vessel shells, closely related to the service life of the reactor pressure vessel and the compositional segregation caused by neutron irradiation. This article uses elemental Mn, Ni, and Si as raw materials for smelting alloy samples, employing the vacuum arc melting method to prepare 31 Mn-Ni-Si ternary alloys. The Mn-Ni-Si ternary system is established at an isothermal section of 500 ℃ through techniques such as X-ray diffraction analysis and scanning electron microscopy. The results indicate the presence of seven ternary compounds and 24 equilibrium three-phase regions in the 500 ℃ isothermal section. Notably, since the MnSi phase is a simple cubic alloy phase, Ni will substitute for Mn in the MnSi phase in the Mn-Ni-Si alloy, thereby forming a solid solution with a larger solubility.

1. Introduction

The Reactor Pressure Vessel (RPV) is an irreplaceable core safety component of nuclear power plants, typically made from low-alloy steel with a low-temperature brittle bcc structure[1]. During its service life, RPV materials exhibit radiation embrittlement due to high-energy neutron irradiations (E > 1 MeV) present in the operating environment, which leads to a continuous decline in their performance. This radiation embrittlement is characterized by an increase in the ductile-brittle transition temperature (DBTT), a decrease in upper shelf energy (USE), and a reduction in fracture toughness (K_{JC}). When radiation embrittlement causes the fracture toughness to drop below the acceptable structural limits, brittle fracture occurs. Therefore, the assessment of the integrity of the RPV hinges on addressing the critical challenge of material radiation embrittlement[2]. Based on extensive observations from microscopic structural experiments, the mechanisms of radiation embrittlement have been summarized internationally into several physical processes due to three changes in microscopic structures: 1) the creation of stable matrix defects induced by radiation, including vacancies, interstitial atoms, dislocation loops, clusters of vacancies or interstitial atoms,

and vacancy-interstitial pairs; 2) the formation of Cu-rich precipitates resulting from radiation, which typically contain alloying elements such as P, Ni, Mn, and Si; and 3) segregation of P near grain boundaries. Currently, efforts to improve the resistance of RPV materials to radiation embrittlement primarily involve reducing the content of harmful alloying elements such as Cu and P[3].

Currently, the nuclear power plants under construction and planned in our country predominantly utilize Pressurized Water Reactor (PWR) technology. The design of the nuclear reactor pressure vessel is crucial to the entire nuclear power construction project, serving as the 'heart' of the reactor. The nuclear reactor pressure vessel (RPV) is a critical component of the nuclear power station. Given the long-term operation in harsh environments characterized by high temperature, high pressure, neutron irradiation, thermal aging, corrosion, and fatigue, the performance requirements for the steel used in the reactor pressure vessel have been elevated to a higher standard[4]. Since the discovery of reheat cracking in the A508-II weld overlay in Western Europe in 1970, which led to poor irradiation resistance in the longitudinal welds of pressure vessels, the shaping process for the complete pressure vessel has been altered to overall ring forging, evolving into the A508-III steel that is widely used today[5].

The Mn-Ni-Si ternary alloy system is an important alloy system in the steel used for reactor pressure vessels, and it has a significant impact on the embrittlement of materials due to component segregation resulting from neutron irradiation in pressure vessels. Currently, there is ample research related to the Mn-Ni-Si ternary system, especially in the high temperature range, where the thermodynamic data is relatively rich. However, many of the thermodynamic data are dated, and the rapid development of the nuclear energy field has prompted numerous research teams to study the isothermal sections of this system since the 21st century. In 2011, Hu et al.[6] conducted a study of the isothermal section of the Mn-Ni-Si ternary system at 1000 ℃ using X-ray diffraction analysis (XRD) and SED/EDX experimental analytical methods, while also employing CALPHAD technology to establish the thermodynamic model of this system, and calculating its isothermal section at 800 ℃ through thermodynamic optimization methods. That same year, Liang[7] experimentally determined the isothermal section of this system at 900 ℃ and provided the equilibrium phase diagram of the Mn-Ni-Si system at that temperature, discovering a new ternary compound with a composition approximately equal to $Mn_{45}Ni_{40}Si_{15}$, and noting the absence of the W phase observed by Hu et al. In 2013, Ling[8] investigated and measured the isothermal section of this system at 600 ℃ and provided the equilibrium phase diagram of the Mn-Ni-Si system at this temperature.

Regarding the Mn-Ni-Si system, there is already a considerable amount of literature available. However, due to the presence of multiple ternary phases in this system and the observation from existing literature that the precipitated phases vary at different temperatures, a more comprehensive isothermal section analysis is required to understand the phase precipitation under various conditions. Considering the actual operating temperature of the reactor pressure vessel, this study focuses on the isothermal section of the ternary system at 500 ℃. Research on this related system will provide scientific basis and thermodynamic data for the composition design of nuclear structural steels and high-performance steel materials.

2. Experimental Methods

All samples were prepared using electrolytic manganese (99.8 wt.%), metallic nickel (99.9 wt.%), and high-purity silicon (99.99 wt.%). Each alloy sample weighed 2 g, with a precision of 0.001 g. The alloy specimen materials were arc melted in a high-purity argon (99.999 wt.%) atmosphere. Before melting the alloy samples, metallic zirconium was first melted and placed in the center of

the arc furnace to absorb residual oxygen in the furnace. To ensure uniformity in the internal composition of the melted alloy, all alloy samples needed to be stirred and flipped after one melting process, with the melting cycle repeated at least five times, each lasting between 30 seconds and 2 minutes. The weight loss of all alloy samples after melting did not exceed 1%. The melted alloy samples were sealed in vacuum quartz tubes and placed in a heat treatment furnace for diffusion annealing. After annealing, the vacuum quartz tubes containing the sealed samples were quickly removed from the heat treatment furnace and plunged into cold water for quenching, allowing us to obtain a high-temperature structure in a balanced state. Subsequently, the alloy specimens of this system were cut into pieces; some were powdered, while others were prepared for metallographic samples through embedding, grinding, and polishing. To determine the phase composition of the alloy samples, the powdered samples were analyzed using X-ray diffraction (XRD) with a Bruker Advance-D8 diffractometer, utilizing CuKa radiation at 40 kV and 40 mA. The prepared metallographic samples were then examined using a scanning electron microscope (SEM, EVO18) equipped with an energy dispersive spectrometer to observe the microstructure of the alloy compositions after annealing, with the composition values of each phase being the average of five independent measurements. The original composition and phase analysis results of the alloy samples involved in this study are shown in Table 1.

Table 1 The original composition and phase analysis results of the alloy sample.

No.	Nominal (at. %)			Phase analysis	Space group	Phase compositional (at. %, SEM)		
	Mn	Ni	Si			Mn	Ni	Si
1	40	45	15	Mn_2Ni_3Si	$Fd\bar{3}m$	36.8	46.5	16.7
				γMnNi	$Fm\bar{3}m$	53.7	42.8	3.5
2	42	48	10	Mn_2Ni_3Si	$Fd\bar{3}m$	37.3	52.4	10.3
				γMnNi	$Fm\bar{3}m$	50.1	44.6	5.3
3	25	55	20	Mn_2Ni_3Si	$Fd\bar{3}m$	35.6	50.9	13.5
				$Mn_6Ni_{16}Si_7$	$Fm\bar{3}m$	19.8	60.9	19.3
4	28	44	28	Mn_2Ni_3Si	$Fd\bar{3}m$	34.9	42.3	22.8
				$Mn_6Ni_{16}Si_7$	$Fm\bar{3}m$	20.1	52.8	27.1
5	32	36	32	$Mn_3Ni_3Si_2$	$P6_3/mmc$	38.1	36.7	25.2
				MnNiSi	$Pnma$	33.5	35.7	30.8
6	48	32	20	Mn_3Ni_2Si	$Fm\bar{3}m$	45.4	34.9	19.7
				—	—	59.9	23.8	16.3
7	15	60	25	$Mn_6Ni_{16}Si_7$	$Fm\bar{3}m$	21.1	54.8	24.1
				$Ni_{31}Si_{12}$	$R\bar{3}$	1.8	72.1	26.1
8	10	45	45	$MnNi_4Si_3$	$P6/mmm$	17.8	37.9	44.3
				Ni_3Si_2	$Fm\bar{3}m$	8.7	50.6	40.7
9	12	70	18	$Mn_6Ni_{16}Si_7$	$Fm\bar{3}m$	16.2	65.4	18.4
				Ni_3Si	$Pm\bar{3}m$	2.8	74.3	22.9
				γMnNi	$Fm\bar{3}m$	12.9	75.2	11.9
10	5	60	35	Ni_2Si	$P6_3/mmc$	2.7	64.7	32.6
				Ni_3Si_2	$P6_3/mcm$	8.3	55.9	35.8
11	18	50	32	$Mn_6Ni_{16}Si_7$	$Fm\bar{3}m$	20.9	49.6	29.5
				Ni_2Si	$Fm\bar{3}m$	16.4	53.7	29.9
12	20	35	45	$MnNi_4Si_3$	$P6/mmm$	13.4	52.1	34.5
				MnSi	$P2_13$	33.4	21.7	44.9
13	25	40	35	MnNiSi	$Pnma$	28.7	39.7	31.6
				$MnNi_4Si_3$	$P6/mmm$	26.3	28.9	44.8
14	30	30	40	MnNiSi	$Pnma$	24.7	42.8	32.5
				Mn_5Si_3	$P6_3/mcm$	50.5	16.4	33.1
				MnSi	$Fd\bar{3}m$	41.7	12.8	45.5
15	35	55	10	Mn_2Ni_3Si	$Fd\bar{3}m$	32.4	56.7	10.9
				γMnNi	$Fm\bar{3}m$	40.9	56.7	2.4
16	38	24	38	MnNiSi	$Pnma$	33.9	37.6	28.5
				MnSi	$Fm\bar{3}m$	41.1	15.7	43.2
				Mn_5Si_3	$P6_3/mcm$	54.4	11.7	33.9
17	55	6	39	MnNiSi	$Pnma$	36.4	32.5	31.1
				MnSi	$P2_13$	50.4	5.2	44.4
				Mn_5Si_3	$P6_3/mcm$	62.1	4.8	33.1

18	57	12	31	$Mn_{55}Si_{25}Ni_{20}$	—	57.1	20.8	22.1
19	58	24	18	Mn_5Si_3 Mn_3Ni_2Si	*P6₃/mcm* *Fm$\bar{3}$m*	64.8 53.4	3.4 28.3	31.8 18.3
				αMn	*I4/mmm*	75.2	10.4	14.4
20	35	35	30	$Mn_3Ni_3Si_2$	*P6₃/mmc*	36.9	34.8	28.3
				MnNiSi	*Pnma*	37.2	33.2	29.6
21	32	16	52	MnSi	*P2₁3*	42.2	12.1	45.7
				$NiSi_2$	*Fm$\bar{3}$m*	6.2	33.9	59.9
22	60	15	25	$Mn_{55}Si_{25}Ni_{20}$	—	56.9	20.7	22.4
				αMn	*I4/mmm*	78.8	0.3	20.9
23	7	43	50	Ni_3Si_2	*Cmc2₁*	4.2	58.7	37.1
				NiSi	*Pnma*	2.5	51.9	45.6
24	8	30	62	MnSi	*P2₁3*	21.2	26.6	52.2
				NiSi	*Pnma*	6.6	45.1	48.3
				$NiSi_2$	*Fm$\bar{3}$m*	10.8	31.9	57.3
25	6	50	44	Ni_3Si_2	*Cmc2₁*	7.4	51.3	41.3
				MnSi	*P2₁3*	15.6	32.8	51.6
				NiSi	*Pnma*	7.7	44.9	47.4
26	46	27	27	Mn_3Ni_2Si	*Fm$\bar{3}$m*	48.3	29.3	22.4
				Mn_5Si_3	*P6₃/mcm*	63.1	4.5	32.4
27	65	27	8	Mn_3Ni_2Si	*Fm$\bar{3}$m*	55.9	32.4	11.7
				αMn	*I4/mmm*	80.4	17.5	2.1
28	38	8	54	MnSi	*P2₁3*	51.2	3.2	45.6
				$Mn_{11}Si_{19}$	*P-4n2*	43.6	0.2	56.2
				(Si)	*Fd$\bar{3}$m*	3.8	2.9	93.3
29	52	24	24	$Mn_{55}Si_{25}Ni_{20}$	—	49.2	28.5	22.3
				Mn_5Si_2	*P41212*	74.1	5.1	20.8
30	44	40	16	Mn_3Ni_2Si	*Fm$\bar{3}$m*	48.3	38.1	13.6
				γMnNi	*Fm$\bar{3}$m*	53.9	42.2	3.9
31	10	52	38	$MnNi_4Si_3$	*P6/mmm*	16.1	41.2	42.7
				Ni_3Si_2	*Cmc2₁*	5.5	59.1	35.4

3. Results and Discussion

Fig. 1(a) shows the backscattered electron image of alloy 3, $Mn_{25}Ni_{55}Si_{20}$, where the coexistence of two phases is clearly observed in the backscattered image. The black region corresponds to the phase $Mn_6Ni_{16}Si_7$(T) and the light gray region corresponds to the phase Mn_2Ni_3Si(Γ_2). This result is consistent with the XRD spectrum analysis, as shown in Fig. 1(b). Therefore, alloy 3 is positioned on the phase equilibrium line of $Mn_6Ni_{16}Si_7$(T) and Mn_2Ni_3Si(Γ_2). For the Mn-Ni-Si system, even after melting and heat treatment, residual liquid phase can still be seen in the backscattered image. Comparing these results with previous experiments, we observe that liquid phase also exists in other isothermal sections; thus, we consider this to be a normal occurrence.

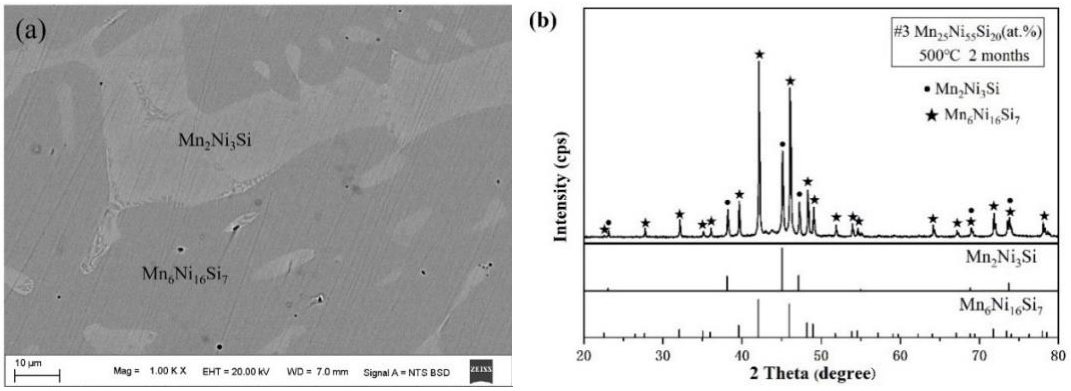

Fig. 1 Experimental results of alloy 3 annealed at 500 ℃ for 2 months, (a) BSE micrograph; (b) XRD patterns.

The equilibrium of MnNiSi and $Mn_3Ni_3Si_2$ phases was observed in alloy 5, composed of $Mn_{32}Ni_{36}Si_{32}$. In the backscattered electron image of Fig. 2(a), the black region corresponds to the

MnNiSi phase, while the light gray region corresponds to the $Mn_3Ni_3Si_2$ phase. The results from X-ray diffraction analysis confirm the presence of these two phases in alloy 5, consistent with the observations made in the backscattered electron image, as shown in Fig. 2(b). Based on the analytical results, it can be concluded that alloy 5 is composed of both the MnNiSi and $Mn_3Ni_3Si_2$ phases.

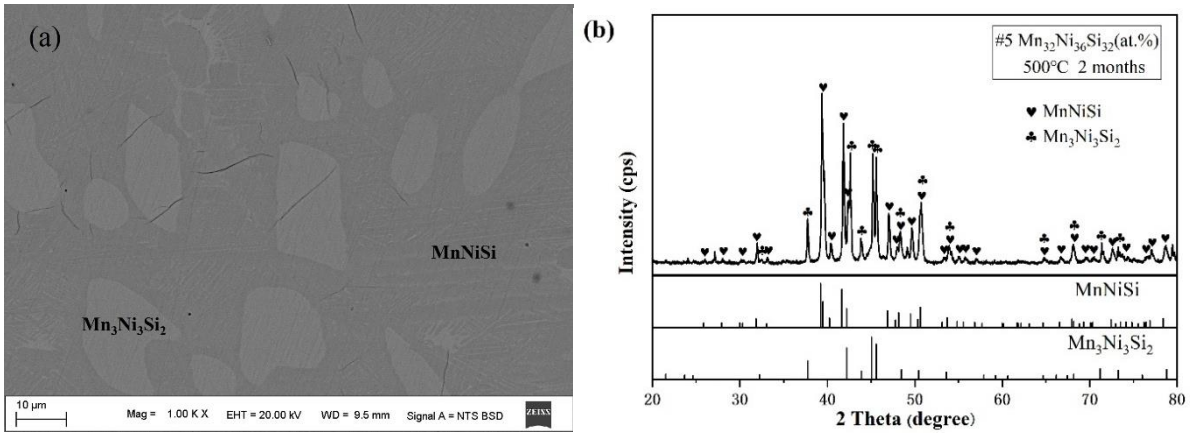

Fig. 2 Experimental results of alloy 5 annealed at 500 ℃ for 2 months, (a) BSE micrograph; (b) XRD patterns.

As shown in Fig. 3(a) and Fig. 3(b), the backscattered images and XRD analysis results of alloy 9, $Mn_{12}Ni_{70}Si_{18}$, are presented. The backscattered electron images reveal that alloy 9 is composed of three phases. Through X-ray diffraction analysis, the three phases of alloy 9 have been identified as Ni_3Si in the black region, $Mn_6Ni_{16}Si_7$ in the gray region, and (Ni) in the light gray region. This indicates that alloy 9 is located in the three-phase equilibrium zone of Ni_3Si, $Mn_6Ni_{16}Si_7$, and (Ni), and the results of the XRD analysis are consistent with the compositional analysis. The experimental test and analytical results for this sample indicate that there exists a three-phase equilibrium zone of Ni_3Si, $Mn_6Ni_{16}Si_7$, and (Ni) in the Mn-Ni-Si system.

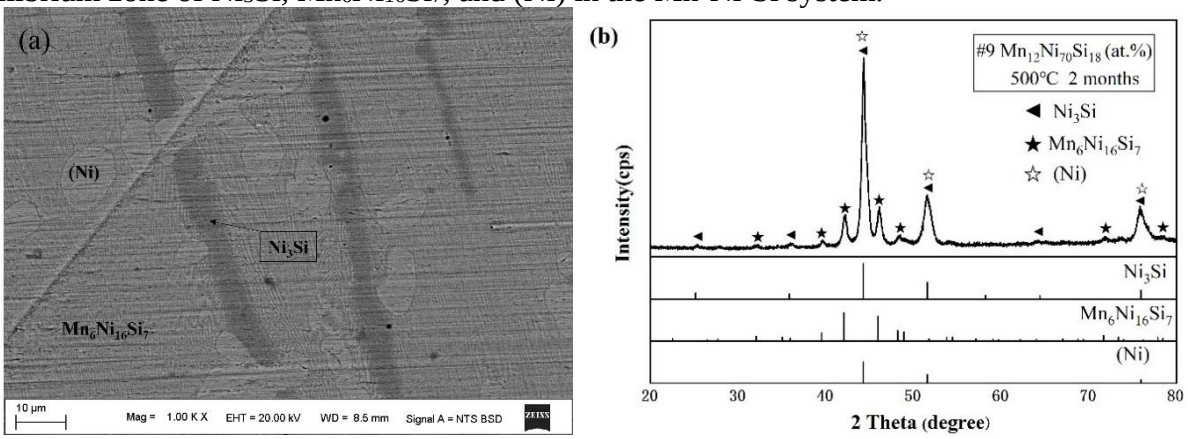

Fig. 3 Experimental results of alloy 9 annealed at 500 ℃ for 2 months, (a) BSE micrograph; (b) XRD patterns.

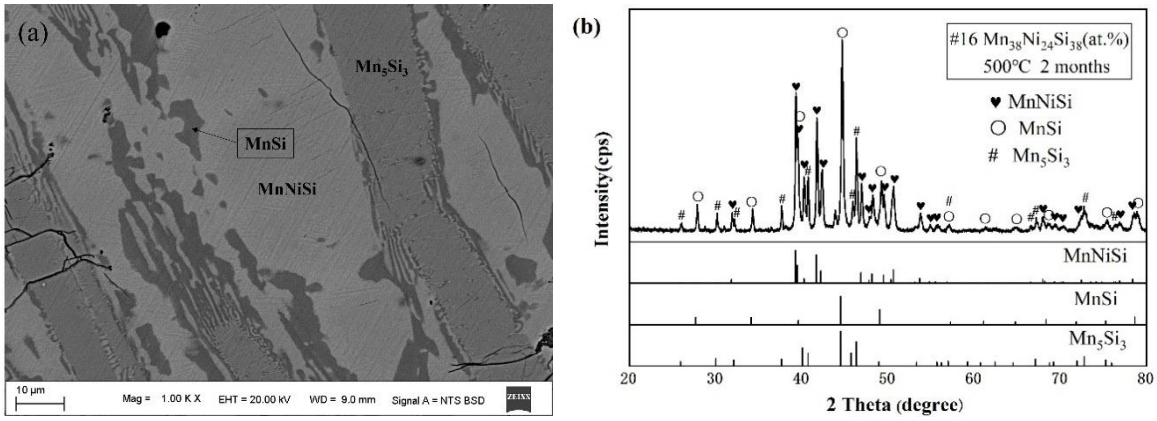

Fig. 4 Experimental results of alloy 16 annealed at 500 ℃ for 2 months, (a) BSE micrograph; (b) XRD patterns.

As shown in Fig. 4(a), the backscattered image of alloy 16 $Mn_{38}Ni_{24}Si_{38}$, subjected to a 500 ℃ annealing treatment for 2 months, reveals the coexistence of three-phase equilibrium: MnSi, MnNiSi, and Mn_5Si_3. Fig. 4(b) presents data from X-ray diffraction analysis, which confirms the results observed in the backscattered electron imagery. It has been determined that in alloy 16, a three-phase equilibrium of MnSi, MnNiSi, and Mn_5Si_3 exists under isothermal conditions at 500 ℃. Due to the compositional nature of this system, certain defects may appear on the sample surface after melting and annealing, such as pores and cracks; for instance, some black cracks can be observed in Fig. 4(a), which are considered a normal phenomenon of this alloy system. In this alloy sample, the solubility of Ni in the MnSi phase is noted to be 15.7 at.%.

The backscattered electron image of alloy 24 ($Mn_8Ni_{30}Si_{62}$) after a two-month annealing treatment at 500 ℃ reveals the coexistence of the three-phase equilibrium of $NiSi_2$, MnSi, and NiSi, as shown in Fig. 5(a). The results of X-ray diffraction analysis, as illustrated in Fig. 5(b), confirm the accuracy of the observations made in the backscattered electron image. Experimental data indicate that the three-phase equilibrium of $NiSi_2$, MnSi, and NiSi exists in alloy 24 at an isothermal section of 500 ℃. In this alloy sample, the solubility of Ni in the MnSi phase is 26.6 at.%.

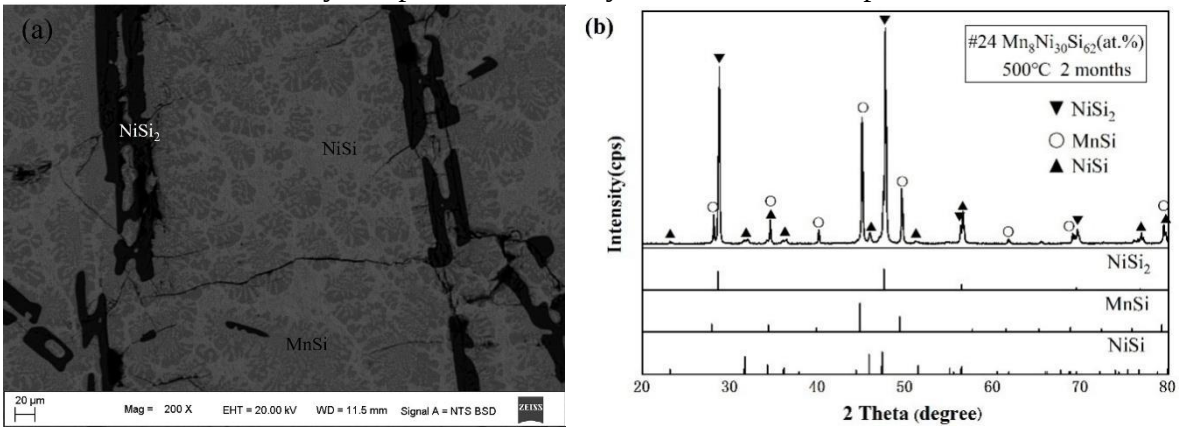

Fig. 5 Experimental results of alloy 24 annealed at 500 ℃ for 2 months, (a) BSE micrograph; (b) XRD patterns.

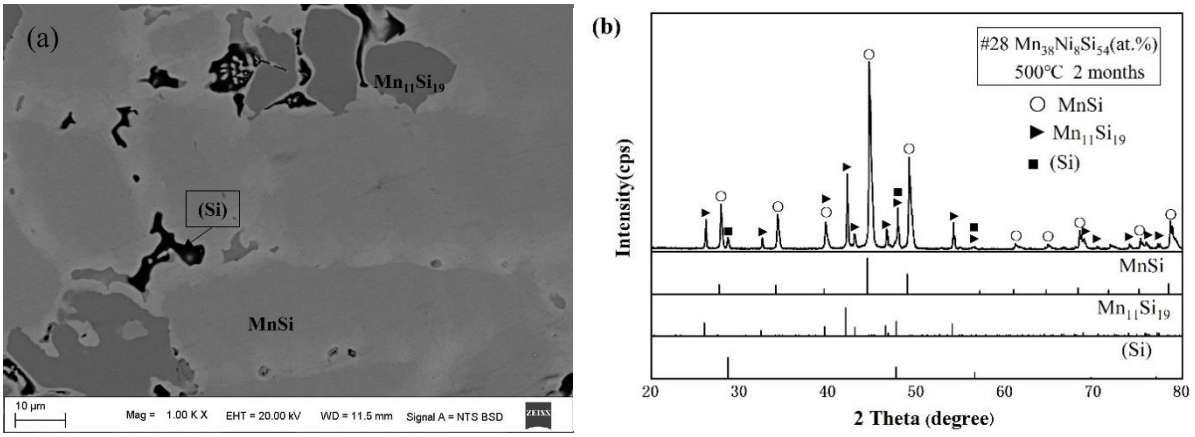

Fig. 6 Experimental results of alloy 28 annealed at 500 ℃ for 2 months, (a) BSE micrograph; (b) XRD patterns.

The backscattered electron images and XRD analysis results of alloy 28 (Mn38Ni8Si54) are shown in Fig. 6. According to the results of the data analysis, the phase of the black regions in the backscatter image is (Si); the phase of the dark gray regions is Mn11Si19; while the phase of the light gray regions is MnSi. The X-ray diffraction results are consistent with the analysis results of the backscatter images, confirming the presence of a three-phase equilibrium of Mn11Si19, MnSi, and (Si) in alloy 28. In this alloy sample, the solubility of Ni in the MnSi phase is 3.2 at.%.Fig. 7(a) shows the backscattered electron image of alloy 25, Mn6Ni50Si44. It can be observed that the alloy is in a three-phase equilibrium. SEM analysis identifies the black phase as MnSi, the gray phase as NiSi, and the light gray phase as Ni3Si2. This is consistent with the analysis results of the XRD spectrum in Fig. 7(b). Both sets of analytical data indicate that alloy 25 is located in the three-phase region of Ni3Si2, MnSi, and NiSi.

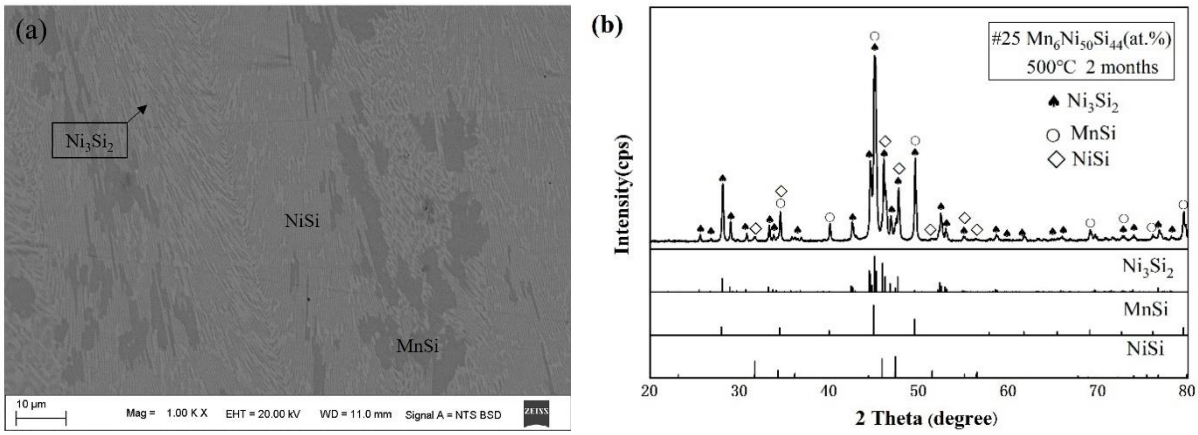

Fig. 7 Experimental results of alloy 25 annealed at 500 ℃ for 2 months, (a) BSE micrograph; (b) XRD patterns.

The isothermal section of the Mn-Ni-Si ternary system at 500 ℃ was determined using 31 alloy samples for analysis. Based on the results, it can be confirmed that $Mn_6Ni_{16}Si_7$(T), $Mn_3Ni_3Si_2$(Γ_1), Mn_2Ni_3Si(Γ_2), MnNiSi(E), Mn_3Ni_2Si(Ω), and $MnNi_4Si_3$(N) remain stable at 500 ℃ compared to the isothermal sections at 800 ℃, 900 ℃, 1000 ℃, and 600 ℃. However, in this experiment, no observation of the two ternary compounds $Mn_{61}Ni_{12}Si_{27}$(R) and $Mn_{66}Ni_4Si_{30}$(U) was made, which is consistent with the findings at 900 ℃, 1000 ℃, and 600 ℃ isothermal sections. Additionally, like Ling's observations in the 600 ℃ isothermal section, we did not observe the compound $Mn_{15}Ni_{50}Si_{35}$(Φ) noted at 800 ℃, 900 ℃, and 1000 ℃ isothermal sections. In this investigation, the

new phase τ discovered by Liang in the 900 ℃ isothermal section and the W phase $Mn_{66}Ni_{20}Si_{14}$ mentioned by Bardos in the 1000 ℃ isothermal section were also not observed.

The MnSi phase is a simple cubic alloy phase, in which Ni substitutes for Mn in the Mn-Ni-Si alloy, forming a solid solution. From this study, it is known that the maximum solubility of Ni in MnSi is 26.6 at.%.

According to the above experimental analysis, the isothermal cross-section of the Mn-Ni-Si ternary system at 500 ℃ is shown in Fig. 8, and it is inferred that there are 24 three-phase equilibrium zones in the ternary system through experiments and phase equilibrium region rules.

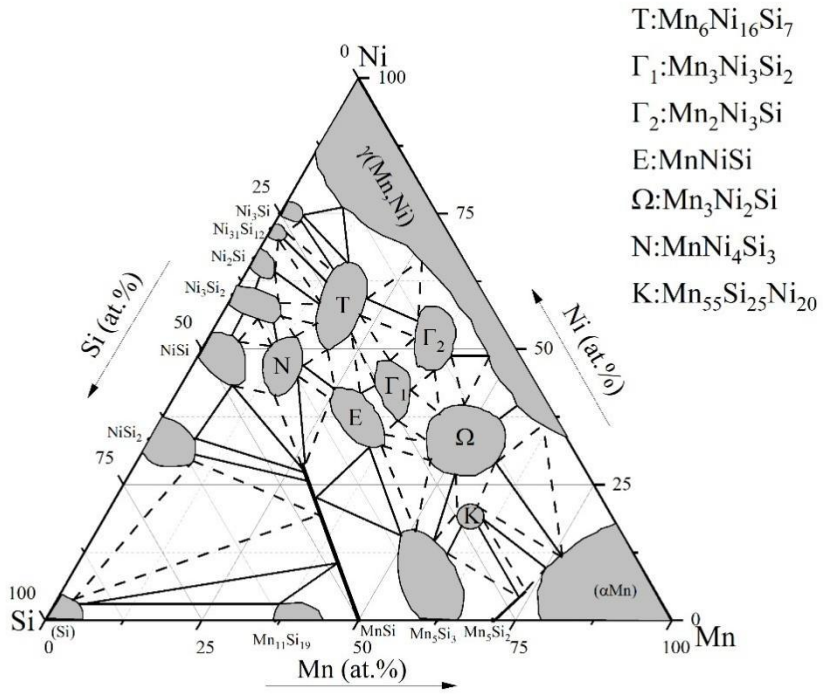

Fig. 8 Isothermal cross-section of Mn-Ni-Si ternary system at 500 ℃

4. Conclusion

The isothermal section of the Mn-Ni-Si ternary alloy system at 500 ℃ was established using X-ray diffraction analysis, scanning electron microscopy, and compositional analysis. This study indicates that at this temperature section:

(1) There are 24 three-phase equilibrium zones in the Mn-Ni-Si ternary system.

(2) From the experimental results, we can observe the stable presence of $Mn_6Ni_{16}Si_7$(T), $Mn_3Ni_3Si_2$(Γ_1), Mn_2Ni_3Si(Γ_2), MnNiSi(E), Mn_3Ni_2Si(Ω), and $MnNi_4Si_3$(N), while $Mn_{61}Ni_{12}Si_{27}$(R), $Mn_{66}Ni_4Si_{30}$(U), $Mn_{15}Ni_{50}Si_{35}$(Φ), and $Mn_{66}Ni_{20}Si_{14}$(W) were not observed.

(3) The maximum solubility of Ni in the MnSi phase is 26.6 at. %.

Acknowledgement

2022 Guangxi Higher Education Institutions Young and Middle-aged Teachers' Scientific Research Basic Ability Improvement Project (2022KY0150)

2024 Guangxi University for School-level Research Project (2023MDKJ006)

References

[1] Yang W D. Reactor Materials Science [M]. Atomic Energy Press, 2006.
[2] Lin H, Zhong W H, Tong Z F, Ning G S, Zhang C Y, Yang W. Irradiation embrittlement behavior and prediction of pressure vessels of domestic reactors[J]. Atomic Energy Science and Technology, 2021, 55: 1170–1176.
[3] Qiao J S, Yang W. Research progress on irradiation embrittlement mechanism of reactor pressure vessel materials[J]. Atomic Energy Science and Technology, 2012, 46: 480–486.
[4] Chen S G. Steel for reactor pressure vessels in nuclear power plants and manufacturing processes[J]. Large castings and forgings, 1994, 02: 25–34.
[5] Tong Z F, Ning G S, Zhang C Y, Yang W, Bai B. Research on irradiation embrittlement behavior and prediction technology of reactor pressure vessel steel[J]. Annual report of China Institute of Atomic Energy, 2016, 1: 2.
[6] HU B, XU H, LIU S, et al. Experimental investigation and thermodynamic modeling of the Mn–Ni–Si system[J]. Calphad, 2011, 35(3): 346-354.
[7] Liang J L, Phase equilibrium and crystal structure of key ternary systems of Zn-Mn-Ni-Sn-Si system[D]. Central South University, 2011.
[8] Ling M R, Phase diagram of Mn-Si-TM(TM=Ni,Zr,Ti) ternary alloy isothermal section at 600 ℃[D]. Guangxi University, 2013.